Int J Adv Manuf Technol (2017) 93:4169–4178
DOI 10.1007/s00170-017-0850-8

ORIGINAL ARTICLE

External aerodynamic force on an ultra-precision diamond fly-cutting machine tool for KDP crystal machining

Liang Liu[1] · **Lihua Lu**[1] · **Qiang Gao**[1] · **Rui Zhang**[1] · **Wanqun Chen**[1]

Received: 14 March 2017 / Accepted: 20 July 2017 / Published online: 3 August 2017

Abstract In the ultra-precision fly-cutting machine tool, the speed of the spindle is very high and the distance between the tool holder and the workpiece is small. There will be normal aerodynamic forces below the tool holder and on the workpiece under the influence of external air. The aerodynamic forces will directly result in the vibration of the machine tool and further affect the surface topography of the workpiece. This paper mainly studies the external aerodynamic forces on a fly-cutting machine tool. It results from the periodical and intermittent sweep between the rotating tool holder and the workpiece. The method of computational fluid dynamics (CFD) is adopted to study this phenomenon. Besides, the aerodynamic forces at different spindle speeds are compared. With the increase of the spindle speed, the amplitude and mean value of the aerodynamic force grows regularly. The aerodynamic forces on the slide and below the tool holder when the cutter processes different regions is presented. The aerodynamic force on the slide shows different behaviors at different machining positions along the feed direction. However, the aerodynamic force below the tool holder is identical. The simulated aerodynamic force on the workpiece is well coincident with the experiment results.

Keywords Fly-cutting machine tool · External aerodynamic force · CFD

✉ Lihua Lu
lulihua2001@163.com

[1] Center for Precision Engineering, Harbin Institute of Technology, Harbin 150001, Heilongjiang, People's Republic of China

1 Introduction

In the inertial confinement fusion device, there are plenty of potassium dihydrogen phosphate (KDP) optical components for frequency multiplication and electro-optical switch cells [1–3]. KDP crystal is extremely soft, fragile, anisotropic, and thermally sensitive. At present, KDP crystals processed by fly-cutting machine tool have relatively good surface quality. Whereas the KDP crystal requires fairly flat topography in ICF program, which needs very small not only roughness but also the root mean square (RMS) and the power spectral density (PSD) [4]. The surface topography of the workpiece is generated by the relative vibration between the tool tip and the workpiece. The vibration of the fly-cutting machine tool directly affects the machined surface quality [5–7]. The vibration of the tool tip originates from the spindle vibration excited by external force [8]. Similarly, the vibration of the workpiece is from the slide vibration. Traditionally, cutting force is regarded as the only external exciting force [9–11]. However, in the cutting force test of an ultra-precision fly-cutting machine tool, a suction on the workpiece is clearly observed when the tool holder without cutter sweeps over the workpiece. This suction is actually the aerodynamic force, which results from the external airflow. Yang et al. also found this phenomenon in the experiment, which was just regarded as the effect of airflow disturbance and not studied further [12]. Clearly, the aerodynamic force is an external exciting force that will affect the machining accuracy. Though there are many studies about the effect of the spindle on the machining surface topography [13–16], the external aerodynamic effect on the fly-cutting machine tool is always regarded too slight to be considered and still remains unclear.

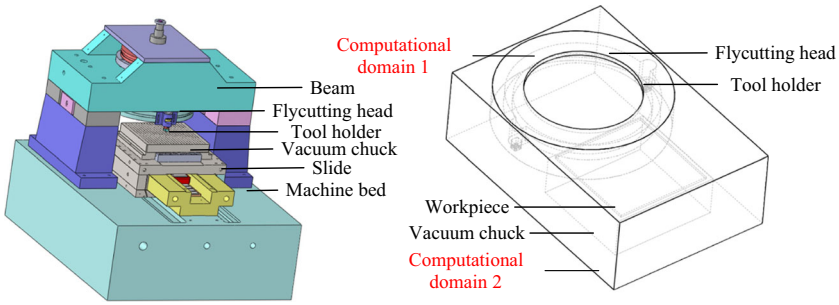

Fig. 1 The fly-cutting machine tool and the model of external air

Table 1 Model dimensions

Rotation radius (mm)	Workpiece dimension (mm)	Vacuum chuck dimension (mm)	Rotation speed (r/min)	Workpiece thickness (mm)	Distance between tool holder and workpiece (mm)
330	430 × 430	480 × 460	390	10	17

The aerodynamic effects on the trains, aircrafts, and racing cars are studied a lot. The vibration of the train is aroused by the lateral aerodynamic force when a high-speed train is traveling into the tunnel, and the force is proportional to the square of the train speed no matter whether there is a reverse cruising train [17]. The amplitudes of the pressure changes in the tunnel and on the train surface are both approximately proportional to the square of the train speed, so are the drags of the train when a train pass through a tunnel [18]. Due to the ground effect, the airflow around the aircraft wings is considerably modified when the plane is taking off or landing, which will result in a sudden change of the aerodynamic force on the wings [19, 20]. The lift of airplane wings will increase when approaching the ground, and the down force of the racing car will increase by the inverted airfoil [21].

Thus, from the existing literature, the aerodynamic force has a large effect on the high-speed object, and the impact will become more complex and dramatic when two relatively moving objects are close. The spindle speed is fast and the distance between the tool holder and the workpiece is close, which is similar to the trains, aircrafts, and racing cars. Besides, with the increase of the workpiece size and processing efficiency, cutting velocity will increase inevitably. The external airflow will become more complex and the impact of external aerodynamic on the machining will become more intense. Therefore, studying the external aerodynamic force is very essential.

This paper focuses on the aerodynamic force below the tool holder and on the slide. Lots of flow simulations are carried out to study its mechanism. Utilizing the data of cutting force experiment on the fly-cutting machine tool, the characteristics of this phenomena can be verified. In order to find the relationship between the spindle speed, and the mean value and the amplitude of aerodynamic force, five spindle speeds of 390, 780, 1170, 1560, and 1950 r/min are calculated.

2 External air model and numerical method

Based on the structure of ultra-precision fly-cutting machine tool, a simplified model of external air is built (Fig. 1). This model removes some small grooves and some other details of the tool holder but retains the pore structure below the tool holder. In order to reduce the computational cost and complexity, the model mainly considers the air around the processing area.

Unstructured tetrahedral mesh for the model is created. The boundary layer prism cells are established to better simulate near-wall flow. As shown in Fig. 1, the model includes two computing domains. The air zone near the fly-cutting head is

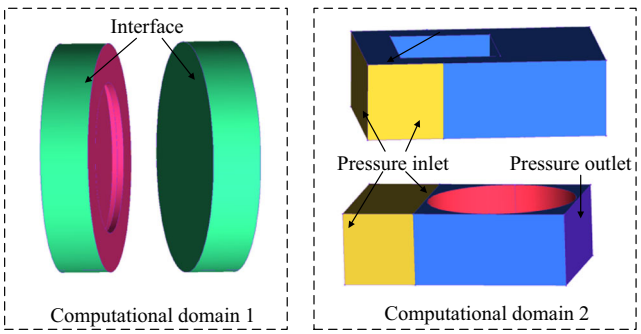

Fig. 2 the boundary conditions of the CFD model

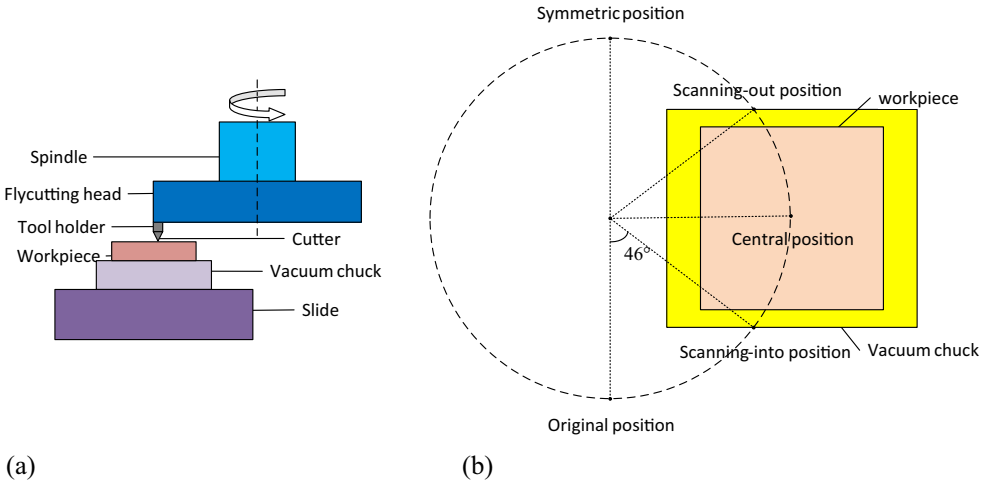

Fig. 3 Processing mechanism: (**a**) the processing principle of machine tool and (**b**) five positions of the path in one circle

the computational domain 1, and the air zone near the workpiece is the computational domain 2. They are meshed respectively. The sliding interface technology is used to solve the relative motion between the tool holder and the workpiece. The moving mesh rotates at the speed of the spindle. The numerical simulations are conducted by using the computational fluid dynamics (CFD) with the software ANSYS Fluent.

Table 1 shows the structure dimension of the external air model. The velocity of tool nose is about 13.5 m/s, so the Mach number of air flow is far less than 0.3. The compressibility of the air can be ignored. The three-dimensional transient, uncompressible Reynolds-averaged Navier–Stokes equations, and SST k-ω turbulence model with curvature correction are employed in the calculations. The equations are solved by the finite-volume method, and the curvature correction can mitigate the overestimation of turbulence level. Because of increasing the boundary layer number can often obtain steady numerical results, the model generates a 10-layer prism mesh to improve the prediction accuracy of the wall boundary layer. The pressure-based solver is used with coupled scheme to address the pressure-velocity coupling to better solve the problem of rotating incompressible flow. The boundary conditions of the CFD model are detailed in Fig. 2. The pressures of the pressure inlet and pressure outlet are 0 Pa.

Figure 3a shows the processing principle of the ultra-precision fly-cutting machine tool. The cutter processes the workpiece with the rotation of the spindle. The vacuum chuck with the workpiece feeds along the slide under the driving linear motor. As shown in Fig. 3b, the tool holder rotates from the original position in the simulation and other positions are the points that are swept over by the tool holder in the following. The aerodynamic forces on the slide (the aerodynamic force on the workpiece and the vacuum chuck) and below the tool holder are concerned.

The residual errors of all variables converge to 5×10^{-5} at each time step. The mesh (it is referred to as the medium mesh) has 3.6 million grid cells. A coarse mesh of 1.4 million grid cells and a fine mesh of 7.1 million grid cells are also generated for the mesh sensitivity study. The simulation results with the time step size of 0.0008 s are a cycle of the aerodynamic forces on the slide (Fig. 4). According to Fig.

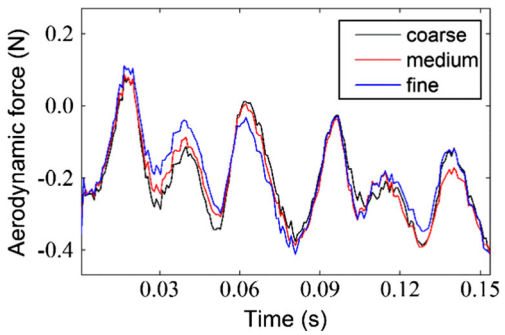

Fig. 4 Comparison of aerodynamic forces on the slide with different meshes

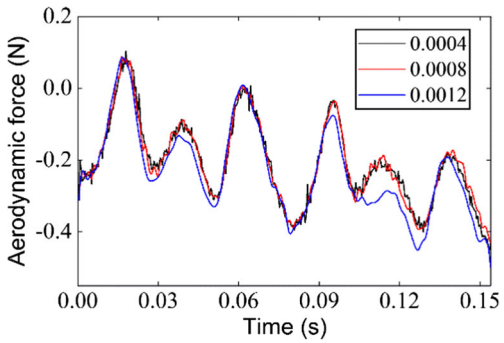

Fig. 5 Comparison of aerodynamic forces on the slide with different time step size

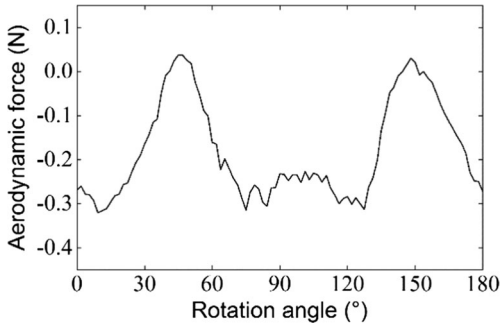

Fig. 6 Aerodynamic force on the slide in a half of circle

4, the results of three kinds of mesh densities are similar. In order to reduce the computational resources and increase the calculation speed, the model adopts medium mesh density.

Respectively, the time step sizes are set as 0.0004, 0.0008, and 0.0012 s for time-independent verification. It can be seen from Fig. 5 that the result of the time step size of 0.0008 s is consistent with the result of 0.0004 s, but there is an obvious deviation from the result of 0.0012 s. The simulation is carried out with the time step size 0.0008 s.

3 Simulation results and discussion

3.1 Aerodynamic force on the slide

There are tool holders that sweep over the workpiece surface in one circle. Take a half of a cycle to analyze the aerodynamic force on the slide because the effects of the two tool holders on the airflow are exactly uniform theoretically. Figure 6 shows the change of aerodynamic force on the slide when the machine tool is processing the center of workpiece along the feed

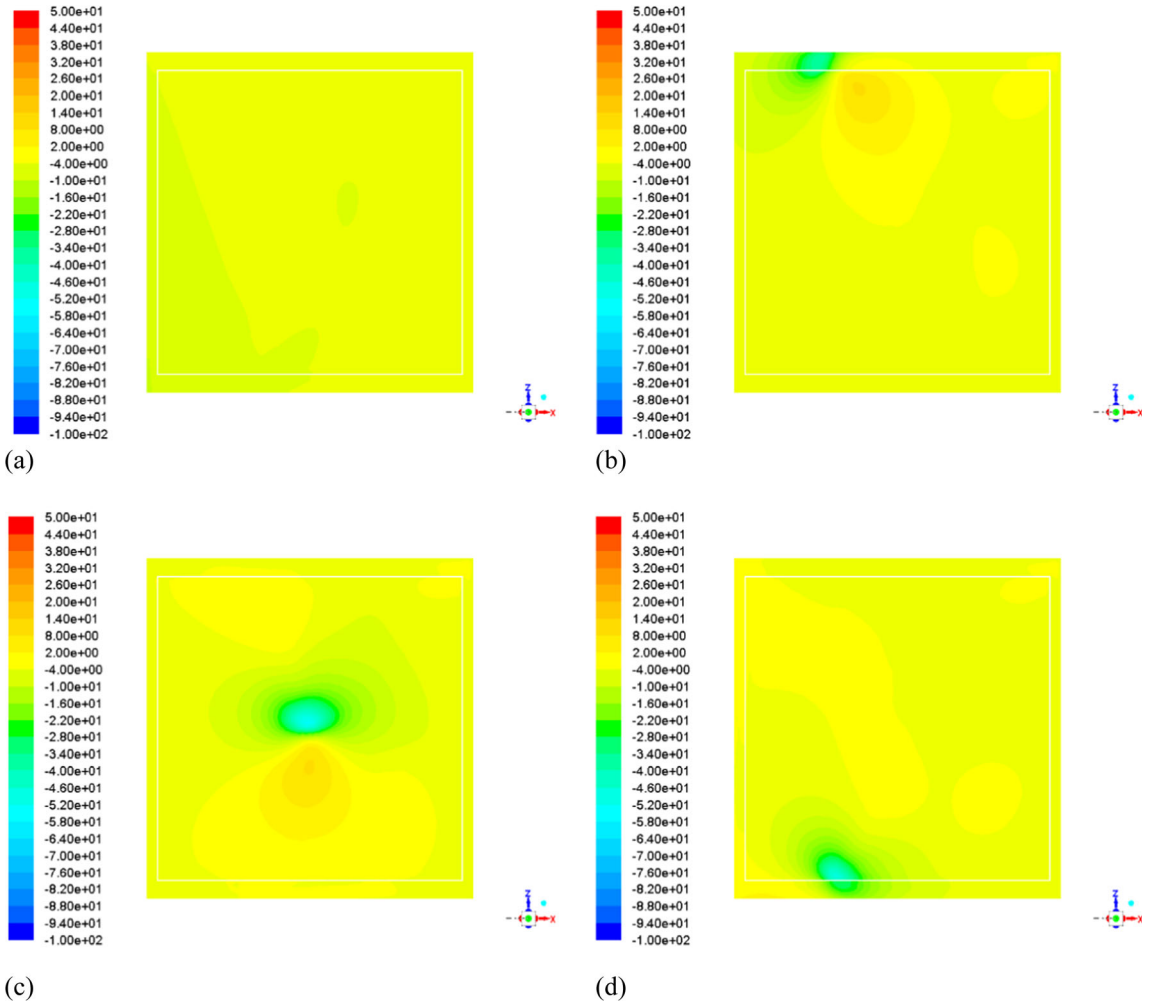

Fig. 7 Pressure profiles on the workpiece and vacuum chuck with different positions of tool holder. **a** Original position. **b** Scanning-into position. **c** Central position. **d** Scanning-out position

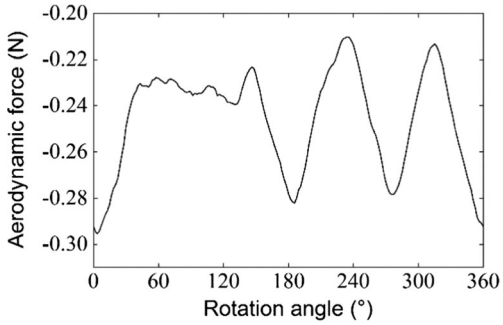

Fig. 8 Aerodynamic force below the tool holder in one circle

direction. The aerodynamic force on the slide experiences three peaks and valleys during a half of circle.

It is distinct to qualitatively figure out the variable characteristics of the aerodynamic force by analyzing the time-varying pressure profiles on the workpiece and vacuum chuck that is shown in Fig. 7. When the tool holder is in the high-speed movement, the air in front of the tool holder is compressed to form a high-pressure zone and the air behind the tool holder forms a negative pressure zone. Figure 7 is the pressure profiles of the workpiece and vacuum chuck when the tool holder sweeps over four positions seen from down to up. As the tool holder gradually approaches the workpiece from the original position, the aerodynamic force on the slide gradually increases because the positive pressure area on the workpiece becomes bigger and bigger. As shown in Fig. 7b, when the tool holder reaches the scanning-into position, the tool holder rotates 46° from the original position and the positive pressure area reaches its maximum, so the aerodynamic force on the slide reaches a maximum value.

As the empty tool holder sweeps over the workpiece, the aerodynamic force on the slide gradually decreases due to the entry of the negative pressure zone behind the tool holder. The aerodynamic force gets to be a minimum when the total negative pressure area just reaches the workpiece completely. As the tool holder continues to sweep over the workpiece, the aerodynamic force on the slide will increase slightly and keep constant generally. With the leaving of the positive pressure area on the workpiece, the aerodynamic force on the slide begins to decline. When the tool holder reaches the scanning-out position, the positive pressure zone has left and the negative pressure zone begins to leave the workpiece; the aerodynamic force on the slide reaches the second minimum (Fig. 7d). Then, with the departure of the negative pressure zone, the aerodynamic force begins to increase and reaches the maximum when the negative pressure area on the workpiece and vacuum disappears completely. Finally, due to the tail vortex, another negative pressure zone arises when the negative pressure zone is completely away from the vacuum chuck. The negative area on the workpiece and vacuum chuck gradually increases and the aerodynamic force gradually reduced until the tool holder reaches the position after the symmetrical position about 10°. Figure 7a shows the pressure profile in the original position. It can be seen that the negative pressure area on the workpiece and vacuum chuck is very clear. Figure 7c shows the pressure profile of the vacuum chuck and the workpiece when the tool holder is sweeping over the central position.

Table 2 Time step sizes with different spindle speeds

Rotation speed(r/min)	390	780	1170	1560	1950
Velocity(m/s)	13.5	27	40.5	54	67.5
Time step size(s)	0.0008	0.0004	0.000267	0.0002	0.00016

3.2 Aerodynamic force below the tool holder

There is also an aerodynamic force below the tool holder when the tool holder sweeps over the workpiece. Aerodynamic force and cutting force as the external exciting force result in the vibration of the spindle, which affects the machined surface topography directly. Figure 8 shows the changing process of aerodynamic force below the tool holder in one period of rotation. It can be seen that the aerodynamic force below the tool holder gradually increases with the tool holder entering the workpiece from the original position, and it reaches a maximum when the tool holder gets to the scanning-into position. As the tool holder sweeps over the workpiece, the aerodynamic force below the tool holder remains approximately constant. The aerodynamic force begins to decrease when the tool holder starts to leave the scanning-

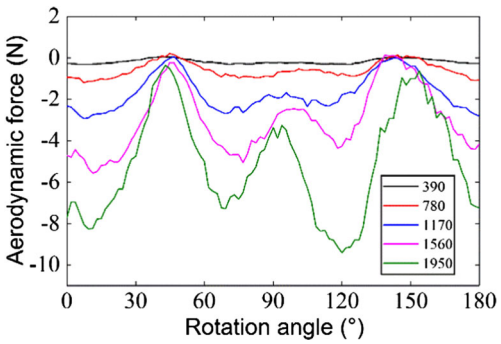

Fig. 9 Comparison of aerodynamic forces on the slide at five rotation speeds

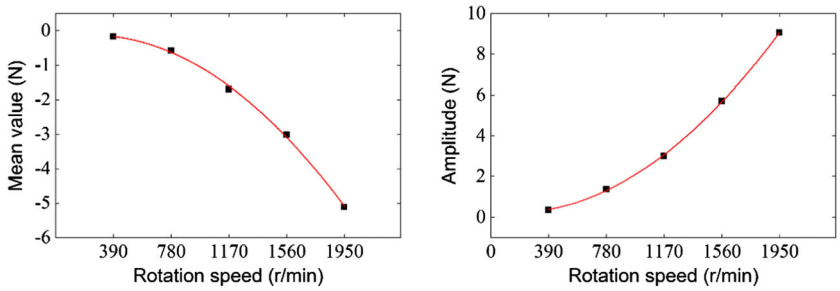

Fig. 10 The mean values and amplitudes of the aerodynamic forces on the slide at five spindle speeds

out position and reaches a minimum in the symmetrical position. There are two peaks and valleys in the latter half of the cycle.

The amplitude of the aerodynamic force on the slide is about 0.35 N, and the aerodynamic force on the lower surface of the tool holder is 0.1 N, which cannot be neglected compared to the cutting force.

3.3 The comparison of aerodynamic forces on the slide at different rotation speeds

The aerodynamic forces on the slide at five speeds are studied. The minimum spindle speed is the spindle speed of the vertical fly-cutting machine tool, and the rest are the multiple of that. To make the calculation accurate, the simulations set different time step sizes so that the tool tip passes the same distance during a time step size at different speeds. The specific spindle speeds and corresponding time step sizes are shown in Table 2.

All the Mach numbers at five speeds are less than 0.3. Therefore, the airflow fields around the tool holder can be approximately regarded as a three-dimensional unsteady incompressible flow field at five speeds. Therefore, the same algorithm will be used at five spindle speeds.

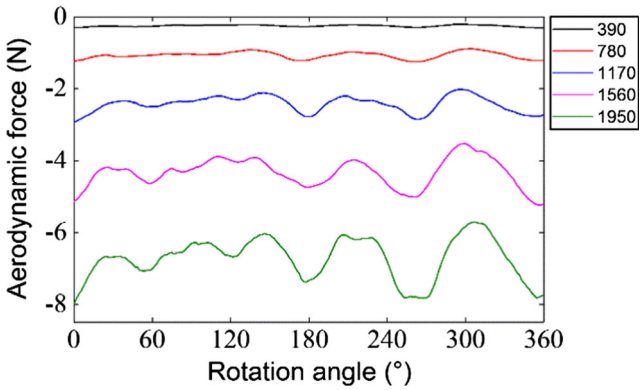

Fig. 11 Comparison of aerodynamic forces on the slide at five rotation speeds

Figure 9 shows five time histories of aerodynamic forces on the slide in a half of circle at five spindle speeds when the tool holder passes the same processing path that goes through the central position of the workpiece in both cut direction and feed direction. At five spindle speeds, the trend of the aerodynamic forces on the slide is uniform. As the spindle speed increases, the absolute value of aerodynamic force increases and aerodynamic change becomes more intense. The mean values and the amplitudes of the aerodynamic forces at different speeds are compared.

Figure 10a gives the mean values of the aerodynamic forces on the slide at five spindle speeds. The fitted equation between the mean value of aerodynamic force y_1 and the spindle speed x is shown as Eq. (1). It can be seen that there is a quadratic function relationship between the mean value of aerodynamic force on the slide and the spindle speed.

$$y_1 = -1.69 \times 10^{-6}x^2 + 8.04 \times 10^{-4}x - 0.23 \quad (1)$$

Figure 10b gives the amplitudes of the aerodynamic forces on the slide at five spindle speeds. The fitted equation between the amplitude of aerodynamic force y_2 and the spindle speed x is shown as Eq. (2). There is a quadratic function relationship between the amplitude of aerodynamic force on the slide and the spindle speed.

$$y_2 = 2.70 \times 10^{-6}x^2 - 7.53 \times 10^{-4}x + 0.26 \quad (2)$$

With the increase of the spindle speed, the term and the constant can be ignored compared with the quadratic term as spindle speed increases in the fitted equation. Therefore, the mean value and the amplitude of aerodynamic force is proportional to the square of the spindle speed with the increase of spindle speed, which is similar to the relationship between the aerodynamic force and the velocity when a high-speed rail is entering a tunnel [13, 14].

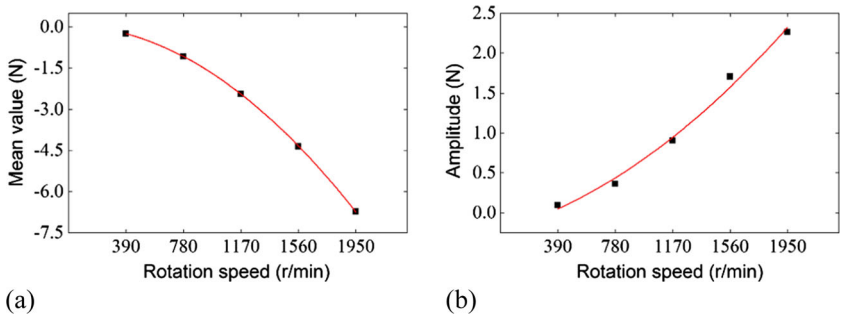

Fig. 12 Mean values and amplitudes of the aerodynamic forces on the slide at five spindle speeds

3.4 The comparison of aerodynamic forces below the tool holder at different rotation speeds

Figure 11 shows a circle of time histories of aerodynamic forces below the tool holder at five spindle speeds when the tool holder passes the same processing path that goes through the central position of the workpiece in both cut direction and feed direction. At different speeds, the trends of the aerodynamic forces are similar. With the increase of the spindle speed, the absolute value of aerodynamic force increases and the aerodynamic change becomes more intense. The mean values and the fluctuation magnitudes of aerodynamic forces below the tool holder at different speeds are compared below.

Figure 12a gives the mean values of the aerodynamic forces below the tool holder at five spindle speeds. The fitted equation between the mean value of aerodynamic force y_3 below the tool holder and the spindle speed x is shown as Eq. (3). There is a quadratic function relationship between the mean value of the aerodynamic force below the tool holder and the spindle speed.

$$y_3 = -1.73 \times 10^{-6}x^2 - 1.08 \times 10^{-4}x + 0.06 \quad (3)$$

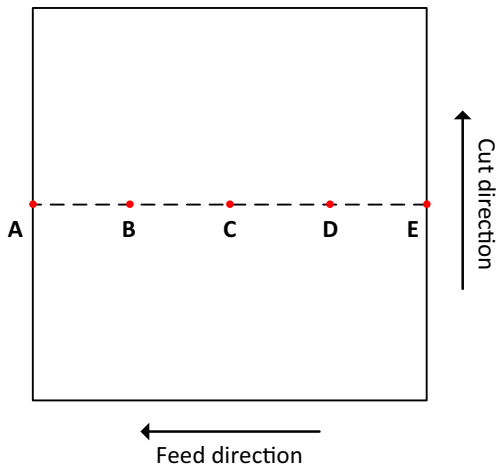

Fig. 13 Five points of the workpiece

Figure 12b gives the amplitudes of the aerodynamic forces below the tool holder at five spindle speeds. There is a quadratic function relationship between amplitude of the aerodynamic force y_4 below the tool holder and spindle speed x:

$$y_4 = 3.93 \times 10^{-6}x^2 + 5.38 \times 10^{-4}x - 0.22 \quad (4)$$

As the spindle speed increases, the mean value and the amplitude of aerodynamic force below the tool holder is also approximately proportional to the square of the spindle speed. Besides, the aerodynamic force will exceed the cutting force when the spindle speed is greater than 1170 r/min.

3.5 The comparison of aerodynamic forces on the slide at different processing positions

Obviously, the aerodynamic forces are completely different when the cutter is machining the workpiece at different locations along the feed direction. The impact of aerodynamic forces on the machined surface topography will be different. Therefore, the analysis of aerodynamic forces when the tool holder sweeps over different locations in the feed direction is necessary. Five special positions are simulated and analyzed to study this question.

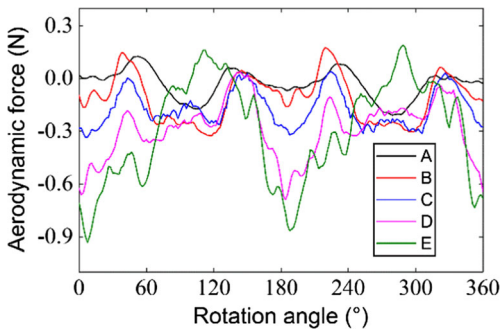

Fig. 14 Comparison of aerodynamic forces on the slide at five machining positions

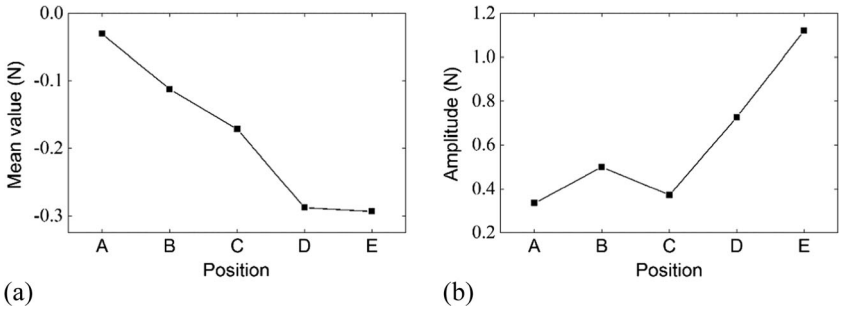

Fig. 15 Mean values and amplitudes of the aerodynamic forces on the slide at five positions

Figure 13 gives five points that is processed as the tool holder sweeps over the workpiece along five paths in the feed direction. Point A is the state when the tool holder first sweeps over the workpiece. Point C is the state when the center of the workpiece is swept. Point E is the state when it sweeps out.

Figure 14 shows the change trends of the aerodynamic forces on the slide during one rotation period when the tool holder sweeps over five machining positions A, B, C, D, and E. The absolute value of the aerodynamic force gradually increases from cutting in to cutting out workpiece along the feed direction. However, the amplitude of the aerodynamic force is not the same.

Figure 15a gives the mean values of the aerodynamic forces on the slide at five machining positions. It can be seen that the mean value gradually reduces with the processing of the workpiece in the feed direction. With the processing of the workpiece, the slide gradually arrives into the middle of the two columns and beam. The inner surface of the columns and the beam greatly affect the airflow, which results in the suction phenomenon on the workpiece becoming more obvious. In addition, the aerodynamic force varies greatly between C and D. Figure 15b shows the amplitudes of the aerodynamic forces on the slide at the five machining positions. The amplitudes of the aerodynamic forces at the five positions are very different. The fluctuation magnitude of the aerodynamic force (1.12 N) at point E is the largest, which is greater than the cutting force.

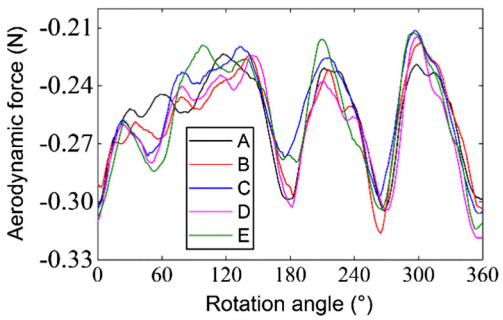

Fig. 16 Comparison of aerodynamic forces below the tool holder at five machining positions

3.6 The comparison of aerodynamic forces below the tool holder at different processing positions

Figure 16 shows the time histories of the aerodynamic forces below the tool holder during one rotation cycle when the tool holder passes through the machining positions A, B, C, D, and E. In the five processing positions, the changes of aerodynamic forces below the tool holder are almost identical.

Figure 17 shows the mean values and amplitudes of the aerodynamic forces below the tool holder.

The mean values and amplitudes of the aerodynamic forces below the tool holder are almost exactly the same in the five machining positions. The amplitudes are about 0.1 N which is about one tenth of the cutting force. However, the impact of aerodynamic force on the vibration of the spindle cannot be ignored because the aerodynamic forces are applied to two tool holders at the same time.

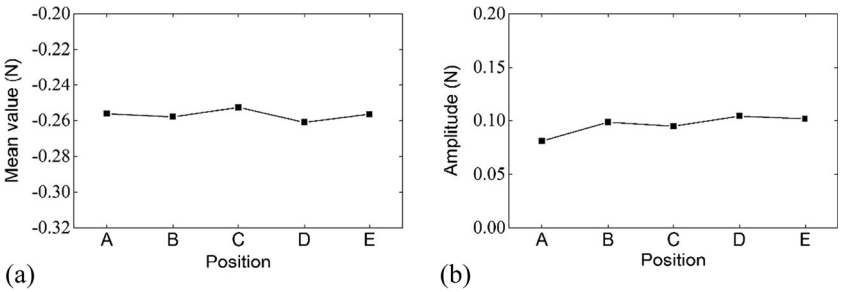

Fig. 17 Mean values and amplitudes of the aerodynamic forces below the tool holder at five positions

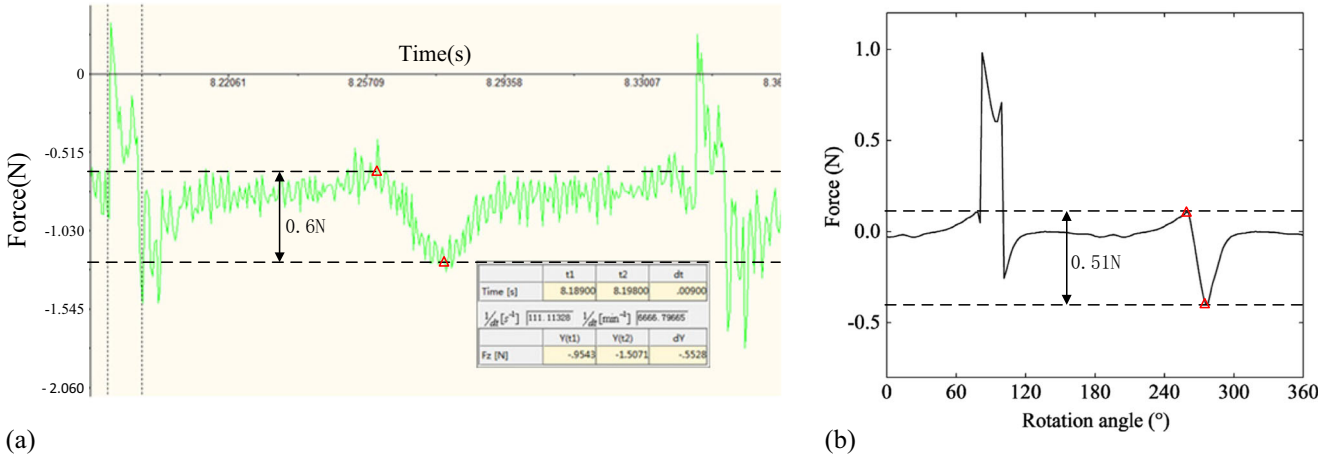

(a) (b)

Fig. 18 The force on the workpiece with the spindle speed of 390 r/min **a** force in the experiment and **b** force in the simulation

4 Experimental confirmation

Two cutting force tests are conducted on a vertical KDP fly-cutting machine tool to verify the correctness of the simulation. To decrease the difficulty of experiment, the workpiece size is taken as 100 × 100 mm and not the original dimension. Two experiments are performed with different cutting parameters. One experiment is performed under spindle speed of 390 r/min and feed rate of 37 μm/r. Another is performed under spindle speed of 260 r/min and feed rate of 18.5 μm/r. Their cutting depths are 10 μm. Figure 18a shows the force measurement on the workpiece with the spindle speed of 390 r/min. According to the experimental results, the value of cutting force is about 1 N. The aerodynamic force on the workpiece is calculated under the workpiece size of 100 × 100 mm. The aerodynamic force on the workpiece plus the cutting force is the simulating force in the first half of the cycle. In the latter half of the cycle, the aerodynamic force remains unchanged. The simulation result of the force on the workpiece is shown in Fig. 18b. It can be seen that the experimental results and the simulation results are almost identical in the latter half of the cycle.

In the experiment, the amplitude of aerodynamic force on the workpiece is about 0.60 N and in the simulation, it is 0.51 N. The error of them is about 15%. The change trend of the force on the workpiece in the first half of the cycle is the same. However, the amplitude of the force in the experiment is larger than that in the simulation when the cutter is processing the workpiece. That is because the cutter has an influence on the aerodynamic force, which is not considered in the simulation.

Figure 19a shows the force measurement on the workpiece with the spindle speed 260 r/min. Figure 19b shows the corresponding simulation result. The amplitude of aerodynamic force in latter half of the cycle is 0.30 N, and the simulation result of the force is 0.23 N. The error of them is about 23.3%. Therefore, the correctness of the simulation is verified well.

Fig. 19 The force measurement on the workpiece with the spindle speed of 260 r/min (**a**) force in the experiment and (**b**) force in the simulation

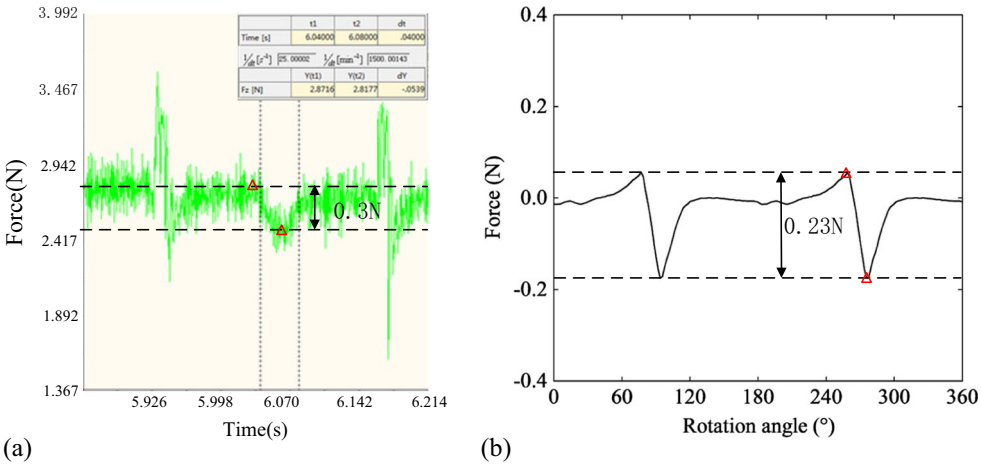

(a) (b)

5 Conclusion and discussion

Via numerical simulation of external aerodynamic force, the following conclusions are made:

1. The amplitudes of aerodynamic forces on the slide and below the tool holder are prominent, of which the influence on the vibration of spindle and slide cannot be ignored.
2. The amplitudes and mean values of the aerodynamic forces on the slide and below the tool holder are approximately proportional to the square of the rotation speed with the increasing of the spindle speed.
3. The amplitudes and mean values of the aerodynamic forces on the slide along the feed direction are very different, and the mean value of the aerodynamic force gradually reduces. However, the aerodynamic force below the tool holder is identical.

Acknowledgments The authors gratefully acknowledge the financial support from the International Science and Technology Cooperation Program of China: Research and Development of High Stiffness Nanodrive Systems of Ultra-precision Machine Tools (2015DFA70630) and the National Science Fund (grant number 51505107).

References

1. Lin ZQ, Deng XM, Fan DY, Wang SJ, Chen SH, Zhu JQ et al (1999) SG-II laser elementary research and precision SG-II program. Fusion Eng Des 44(1):61–66
2. Chen MJ, Pang QL, Wang JH, Cheng K (2008) Analysis of 3D microtopography in machined KDP crystal surfaces based on fractal and wavelet methods. Int J Mach Tools Manuf 48(7):905–913
3. Yoreo JJD, Burnham AK, Whitman PK (2002) Developing KH2PO4 and KD2PO4 crystals for the world's most power laser. Int Mater Rev 47(3):113–152
4. Liang YC, Chen WQ, Bai QS, Sun YZ, Chen GD, Zhang Q, Sun Y (2013) Design and dynamic optimization of an ultraprecision diamond flycutting machine tool for large KDP crystal machining. Int J Adv Manuf Technol 69(1):237–244
5. An CH, Zhang Y, Xu Q, Zhang FH, Zhang JF, Zhang LJ, Wang JH (2010) Modeling of dynamic characteristic of the aerostatic bearing spindle in an ultra-precision fly cutting machine. Int J Mach Tools Manuf 50(4):374–385
6. Miao JG, Yu DP, An CH, Ye FF, Yao J (2016) Investigation on the generation of the medium-frequency waviness error in flycutting based on 3D surface topography. Int J Mach Tools Manuf 90:1–9
7. Chen WQ, Liang YC, Luo XC, Sun YZ, Wang HR (2014) Multi-scale surface simulation of the KDP crystal fly cutting machining. Int J Adv Manuf Technol 73(1):289–297
8. Luo XC, Cheng K, Robert W (2005) The effects of machining process variables and tooling characterisation on the surface generation. Int J Adv Manuf Technol 25(11):1089–1097
9. Chen WQ, Liang YC, Sun YZ, Huo DH, Lu LH, Liu HT (2014) Design philosophy of an ultra-precision fly cutting machine tool for KDP crystal machining and its implementation on the structure design. Int J Adv Manuf Technol 70(1):429–438
10. Zhang SJ, To S, Cheung CF, Wang HT (2012) Dynamic characteristics of an aerostatic bearing spindle and its influence on surface topography in ultra-precision diamond turning. Int J Mach Tools Manuf 62(1):1–12
11. Chen WQ, Lu LH, Yang K, Huo DH, Su H, Zhang QC (2015) A novel machine tool design approach based on surface generation simulation and its implementation on a fly cutting machine tool. Int J Adv Manuf Technol 80(5):829–837
12. Yang X, An CH, Wang ZZ, Wang QJ, Peng YF, Wang J (2016) Research on surface topography in ultra-precision flycutting based on the dynamic performance of machine tool spindle. Int J Adv Manuf Technol 87:1957–1965
13. Khanfir H, Bonis M, Revel P (2005) Improving waviness in ultra precision turning by optimizing the dynamic behavior of a spindle with magnetic bearings. Int J Mach Tools Manuf 45(7–8):841–848
14. An CH, Zhang Y, Zhang FH, Zhang JF, Zhang LJ, Wang JH (2010) Modeling of dynamic characteristic of the aerostatic bearing spindle in an ultra-precision fly cutting machine[J]. Int J Adv Manuf Technol 50(4):374–385
15. Zhang SJ, To S (2013) A theoretical and experimental study of surface generation under spindle vibration in ultra-precision raster milling. Int J Mach Tools Manuf 75(12):36–45
16. Liang YC, Chen WQ, An CH, Luo XC, Chen GD, Zhang Q (2013) Investigation of the tool-tip vibration and its influence upon surface generation in flycutting. Proc Inst Mech Eng 228(12):2162–2167
17. Suzuki M, Ido A, Sakuma Y, Kajiyama H (2008) Full-scale measurement and numerical simulation of flow around high-speed train in tunnel. J Mech Syst Transp Logist 1(1):281–292
18. Li XH, Deng J, Chen DW, Xie FF, Zheng Y (2011) Unsteady simulation for a high-speed train entering a tunnel. J Zhejiang Univ Sci A 12(12):957–963
19. Qu QL, Lu Z, Guo H, Liu PQ (2015) Numerical investigation of the aerodynamics of a Delta wing in ground effect. J Aircr 52(1):329–340
20. Ahmed MR, Takasaki T, Kohama Y (2007) Aerodynamics of a NACA4412 airfoil in ground effect. AIAA J 45(1):37–47
21. Joseph K (2006) Aerodynamics of race cars. Annu Rev Fluid Mech 38(1):27–63